

Generalized Trusted Multi-view Classification Framework with Hierarchical Opinion Aggregation

Long Shi, *Member, IEEE*, Chuanqing Tang, Huangyi Deng, Cai Xu, Lei Xing, *Member, IEEE*, Badong Chen, *Senior Member, IEEE*

Abstract—Recently, multi-view learning has witnessed a considerable interest on the research of trusted decision-making. Previous methods are mainly inspired from an important paper published by Han *et al.* in 2021, which formulates a Trusted Multi-view Classification (TMC) framework that aggregates evidence from different views based on Dempster’s combination rule. All these methods only consider inter-view aggregation, yet lacking exploitation of intra-view information. In this paper, we propose a generalized trusted multi-view classification framework with hierarchical opinion aggregation. This hierarchical framework includes a two-phase aggregation process: the intra-view and inter-view aggregation hierarchies. In the intra aggregation, we assume that each view is comprised of common information shared with other views, as well as its specific information. We then aggregate both the common and specific information. This aggregation phase is useful to eliminate the feature noise inherent to view itself, thereby improving the view quality. In the inter-view aggregation, we design an attention mechanism at the evidence level to facilitate opinion aggregation from different views. To the best of our knowledge, this is one of the pioneering efforts to formulate a hierarchical aggregation framework in the trusted multi-view learning domain. Extensive experiments show that our model outperforms some state-of-art trust-related baselines. One can access the source code on <https://github.com/lshi91/GTMC-HOA>.

Index Terms—multi-view learning, trusted decision-making, hierarchical opinion aggregation, intra-view aggregation, inter-view aggregation,

I. INTRODUCTION

MULTI-VIEW learning has garnered increasing interest due to the prevalence of multi-source data in real-world scenarios. A typical example can be observed in the healthcare field, where a patient’s diagnosis is often made based on multiple types of medical examinations. According to the learning paradigm, multi-view learning methods can be broadly categorized into subspace-based methods [1], [2], graph-based methods [3], [4], and deep neural network-based methods [5], [6], which have found diverse applications in classification [7], clustering [8], recommendation systems [9], among others.

Long Shi, Chuanqing Tang and Huangyi Deng are with the School of Computing and Artificial Intelligence, and also with the Financial Intelligence and Financial Engineering Key Laboratory of Sichuan Province, Southwestern University of Finance and Economics, Chengdu 611130, China (e-mail: shilong@swufe.edu.cn, 223081200012@smail.swufe.edu.cn, 223081200043@smail.swufe.edu.cn)

Cai Xu is with the School of Computer Science and Technology, Xidian University, China (e-mail: cxu@xidian.edu.cn)

Lei Xing and Badong Chen are with the Institute of Artificial Intelligence and Robotics, Xi’an Jiaotong University, Xi’an 710049, China (e-mail: xingl@xjtu.edu.cn, chenbd@mail.xjtu.edu.cn)

Most multi-view methods follow one of two technical routes in their research. The first route argues that focusing on the shared information among views is sufficient to uncover the underlying data structure [10]. The second route seeks both consistent and complementary information [11]. While both technical routes have significantly advanced the accuracy of decision-making, they often neglect the crucial aspect of result reliability, which is particularly important in safety-critical applications.

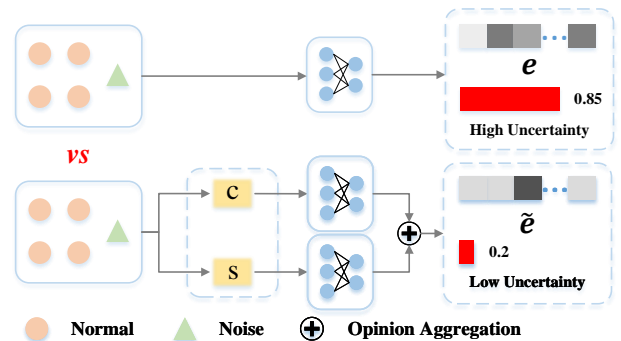


Fig. 1. For a noisy view, evidence directly from a neural network may have high uncertainty, while evidence after intra-view aggregation shows lower uncertainty, thus improving the reliability of view quality.

To address the aforementioned limitation, Han *et al.* proposed an uncertainty-aware Trusted Multi-view Classification (TMC) framework [12]. TMC utilizes the Dirichlet distribution to model the distribution of class probabilities and incorporates the Dempster-Shafer theory [13] to yield a reliable classification result. Inspired by TMC, several subsequent studies have been conducted, focusing on areas such as conflictive opinion aggregation strategy [14], opinion aggregation with evidence accumulation [15], and trusted learning in the presence of label noise [16]. Essentially, these methods can be characterized as following the paradigm of inter-view aggregation, they do not make efforts to investigate the potential benefits of exploiting intra-view information. But we argue that incorporating intra-view information is of significant importance. To explain it intuitively, we provide an example involving noisy multi-view data, as shown in Fig. 1. In such a scene, previous trusted methods produce large uncertainty in classification evidence, while resulting in limited classification accuracy. This observation motivates us to consider a problem: *can we reduce the uncertainty of noisy view data to enhance view quality, thereby improving decision-making accuracy and reliability?*

In response to the aforementioned challenge, we propose a novel trusted learning framework for multi-view data, namely Generalized TMC framework with Hierarchical Opinion Aggregation (GTMC-HOA). In the new framework, we propose a two-phase hierarchical aggregation process: intra-view aggregation and inter-view aggregation. The intra-view aggregation is realized by first learning the common information shared across different views, as well as the unique information specific to each view. Specifically, the common information is acquired by minimizing the confusion adversarial loss, while the view-specific information is obtained by enforcing an orthogonal constraint with respect to the common information. Once both the common and specific information for each view are obtained, we carry out the intra-view aggregation based on Dempster’s rule of combination. This aggregation phase is useful to reduce the uncertainty of evidence in the presence of noisy view, thereby enhancing the quality of each view. Subsequently, the improved views are used to facilitate inter-view aggregation. This aggregation phase involves two procedures. Firstly, an attention mechanism is designed at the level of evidence to extract attention from other views, which circumvents the limitation of previous trusted methods that treat each view equally, thereby further reinforcing evidence reliability. Secondly, we perform the inter-view aggregation. In summary, *we are the first to propose a hierarchical aggregation framework in trusted multi-view learning*, and our main contributions of GTMC-HOA include:

- In the first hierarchy, the intra-view aggregation, we learn both the common and specific components for each view, and then conduct intra-view aggregation. This hierarchy of aggregation stands from the aspect of intra views, which helps to reduce evidence uncertainty, particularly in the presence of noisy data.
- In the second hierarchy, the inter-view aggregation, we first design an attention mechanism at the evidence level to capture information from other views, and then execute inter-view aggregation. This hierarchy of aggregation is constructed from the perspective of inter views, enhancing the quality of evidence and ultimately bolstering decision-making reliability.
- Extensive experiments demonstrate that GTMC-HOA achieves more superior performance than several state-of-art trusted methods.

II. RELATED WORK

In the following, we provide a brief review of representative research in multi-view learning and uncertainty-aware trusted learning.

A. Multi-view Learning

Multi-view learning has seen rapid development in recent years. Multi-view subspace clustering methods receive particular interest because they allow analysis and understanding of data structures in the underlying low-dimensional subspace [11], [17], [18]. Unlike traditional subspace clustering methods that learn self-representation from original features, some latent representation methods were investigated to more

effectively capture comprehensive information among multiple views [19], [20]. The basic idea behind these methods is to project the original features into a latent space, and then learn a latent representation that covers both common and complementary information [21]. Due to the merits of kernel mapping in handling nonlinear structures [22], extensive research has been conducted on kernel-based multi-view methods. In [23], Liu *et al* investigated the issue of incomplete kernel by unifying the procedures of kernel imputation and clustering. By considering the local density of samples, kernel representation capacity can be improved [24]. In addition, tensor-based multi-view subspace learning that is capable of exploiting high-order information demonstrates superiority in capturing the correlations across various views [25]–[27].

Graph techniques also occupy an important position in multi-view learning. Considerable efforts have been devoted to graph-based multi-view clustering [3], addressing specific issues such as consensus graph learning [28]–[30], graph recovering [4], [31], and attributed graphs [32], [33]. With the prosperity of deep learning techniques, scholars are increasingly focusing on incorporating multi-view learning with deep neural networks [34], [35]. Moreover, practical challenges, including but not limited to low-quality views [4], [36] and large-scale data [8], [37], have been extensively studied in the literature.

B. Uncertainty-aware Trusted Learning

However, the aforementioned multi-view learning methods only focus on decision-making accuracy, neglecting the crucial aspect of result reliability, which is important for safety-critical applications. Motivated by evidential deep learning [38] that serves as a representative paradigm for uncertainty estimation, TMC has recently emerged as a significant framework, which utilizes the Dirichlet distribution to model class probability distributions and incorporate the Dempster-Shafer theory to realize trusted classification results [12], [39]. On the basis of TMC, various variants have been developed to address specific issues and enhance performance. Liu *et al.* considered opinion entropy to ensure consistency among multiple views [15]. Xu *et al.* investigated the reliable conflictive multi-view learning problem by designing a conflictive opinion aggregation strategy [14]. Subsequently, they explored schemes to guarantee the reliability of decision-making in scenarios involving noisy labels [16] and semantic vagueness [40]. In [41], Zhou *et al.* examined the potential by incorporating trustworthiness in both early and late fusion stages to enhance prediction quality. More recent advancements on trusted learning can be found in [42]–[45], which covers categories such as semi-supervised learning, multimodal fusion, and open-world learning, among others.

III. METHODOLOGY

In this section, we will introduce our proposed GTMC-HOA in detail, which involves three modules: learning of common and specific information, intra-view aggregation, and inter-view aggregation. The framework of GTMC-HOA is shown in Fig. 2. In this framework, intra-view aggregation is depicted

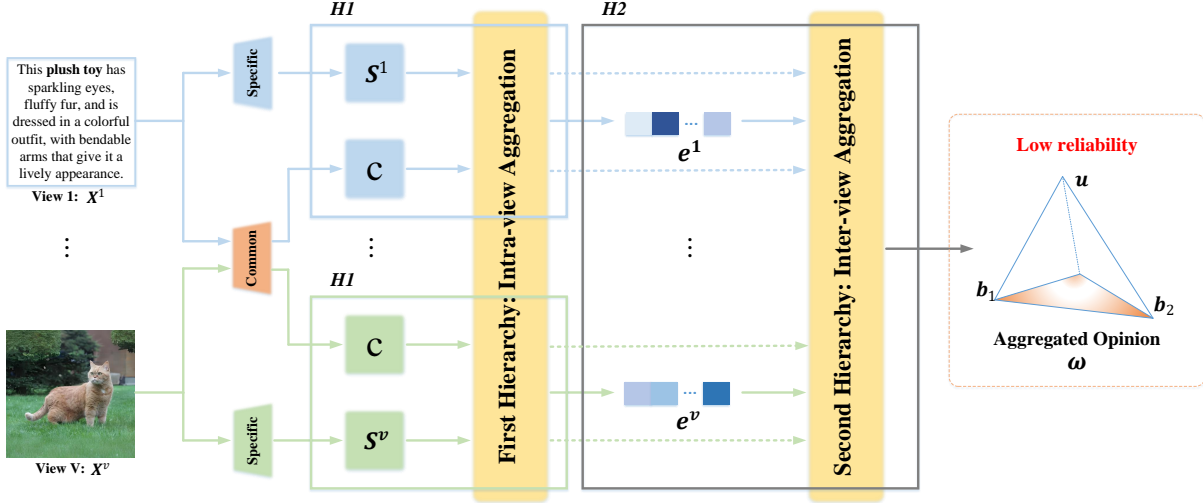


Fig. 2. Illustration of GTMC-HOA. First, we learn the common and specific information for each view. Then, we perform the first-level aggregation, namely intra-view aggregation, to generate high-quality evidence. After obtaining the high-quality evidence of multiple views, we proceed with the second-level aggregation, namely inter-view aggregation, to achieve reliable decision-making results.

in the $H1$ block, while inter-view aggregation is represented in the $H2$ block. For a q -class classification problem, we consider multi-view data $\{\mathbf{X}^i\}_{i=1}^v$ with n samples, where $\mathbf{X}^i = [\mathbf{x}_1^i, \mathbf{x}_2^i, \dots, \mathbf{x}_n^i] \in \mathbb{R}^{d_i \times n}$ represents the i -th view data with d_i dimension.

A. Common and Specific Information

Before implementing the intra-view aggregation, we need to learn both the common and specific information for each view.

Extraction of Common Information: Motivated by [46], we extract the common information by minimizing an adversarial loss \mathcal{L}_{adv} , which serves to confuse the discriminator as to which view the learned common information belongs.

Consider \mathbf{c}_j^i as the common subspace representation of the original i -th view feature \mathbf{x}_j^i from the j -th sample. This representation is extracted using a common subspace extraction layer H_{cse} , such that $\mathbf{c}_j^i = H_{cse}(\phi^i(\mathbf{x}_j^i))$, where $\phi^i(\cdot)$ maps each d_i -dimensional original feature vector into the same l -dimensional space. Define \mathbf{z}_j as the v -dimensional view label vector of \mathbf{c}_j^i , where z_j^i equals 1 and all other elements are 0, indicating that \mathbf{c}_j^i originates from the i -th view. A training set $\mathcal{T}_{adv} = \{(\mathbf{c}_j^i, \mathbf{z}_j) | 1 \leq i \leq v, 1 \leq j \leq n\}$ can be constructed for the discriminator D . The prediction output by D is denoted as $\hat{\mathbf{z}}$, such that $\hat{z}_j = D(\mathbf{c}_j^i)$. The adversarial loss \mathcal{L}_{adv} is then defined as:

$$\mathcal{L}_{adv} = \mathcal{F} \left(- \sum_{j=1}^n \sum_{i=1}^v z_j^i \log(\hat{z}_j^i) \right), \quad (1)$$

where $\mathcal{F}(\cdot)$ is a monotonically decreasing function set to $\mathcal{F}(x) = \exp(-x)$. With this loss function, we are able to confuse the discriminator, preventing it from identifying the true view of the learned subspace representation. Consequently,

the incorporated representation \mathbf{c}_j^i only contains the common information from \mathbf{x}_j^i .

To avoid the unexpected situation that noise may confuse the discriminator, we draw inspiration from [47] and introduce a common subspace multi-view loss \mathcal{L}_{cml} to ensure that \mathbf{c}^i contains certain semantics. Consider a training set $\mathcal{T}_{cml} = \{(\mathbf{c}_j^i, \mathbf{y}_j) | 1 \leq i \leq v, 1 \leq j \leq n\}$ for common subspace representation prediction layer H_{cml} . Let $\hat{\mathbf{y}}$ represent the output by H_{cml} , such that $\hat{y}_j^i = H_{cml}(\mathbf{c}_j^i)$. The loss \mathcal{L}_{cml} can then be defined as:

$$\mathcal{L}_{cml} = - \sum_{j=1}^n \sum_{i=1}^v \sum_{k=1}^q y_{jk} \log(\hat{y}_{jk}^i) + (1 - y_{jk}) \log(1 - \hat{y}_{jk}^i). \quad (2)$$

By incorporating \mathcal{L}_{adv} and \mathcal{L}_{cml} , the overall loss \mathcal{L}_{com} for learning common information can be expressed as:

$$\mathcal{L}_{com} = \mathcal{L}_{adv} + \mathcal{L}_{cml}. \quad (3)$$

Extraction of Specific Information: In an ideal situation, for each view, we aim for the learned common information to be independent of the learned specific information. To achieve this, we enforce an orthogonal constraint on the specific information. Consider \mathbf{s}^i as the l -dimensional feature vector extracted by specific information extraction layer H_{sie} , such that $\mathbf{s}^i = H_{sie}(\mathbf{x}^i)$. We then define the following constraint to encourage orthogonality between \mathbf{s}^i and \mathbf{c} :

$$\mathcal{L}_{spe} = \|(\mathbf{s}^i)^T \mathbf{c}\|_2^2, \quad (4)$$

where $\mathbf{c} = \sum_{i=1}^v \mathbf{c}^i$, and $\|\cdot\|_2$ denotes the l_2 -norm. From the above equation, it is seen that \mathbf{s}^i is orthogonal to $\{\mathbf{c}^1, \dots, \mathbf{c}^v\}$, ensuring that the specific information is as different from the common information as possible.

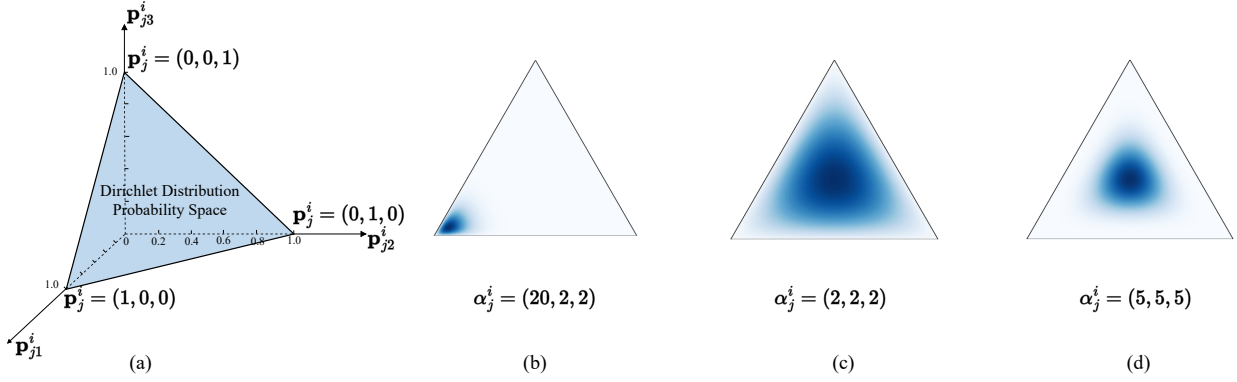


Fig. 3. Examples of Dirichlet distribution and subjective opinion. (a) Possibility space (represented as a standard 2-simplex) for the probability of categories in a three-classification problem. (b)-(d) Prediction cases with different confidence, corresponding to evidence $\mathbf{e}_j^i = \{19, 1, 1\}$, $\mathbf{e}_j^i = \{1, 1, 1\}$, and $\mathbf{e}_j^i = \{4, 4, 4\}$, respectively.

B. Intra-view Aggregation

After obtaining both common and specific information for each view, we execute the first phase of aggregation, namely intra-view aggregation, as shown in Fig. 4. During this phase, we first learn evidence corresponding to the common and specific information by deep neural networks (DNNs), where “evidence” represents metrics collected from the input to support the classification. The theoretical framework of subjective logic (SL) [48] is then employed to associate the parameters of the Dirichlet distribution based on the gathered evidence, thereby obtaining the probabilities of different classes and the uncertainty of decision-making. Finally, opinion aggregation is performed.

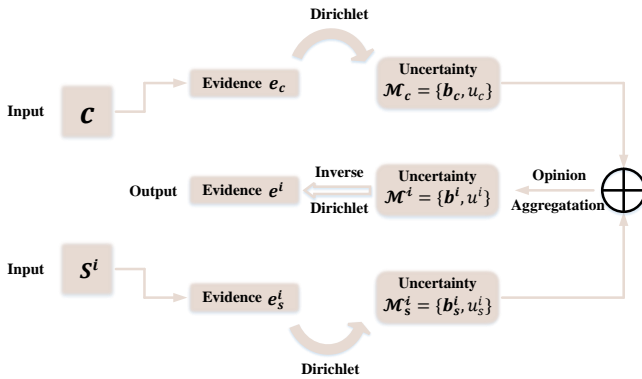


Fig. 4. Structure of intra-view aggregation. The common and specific information of each view are aggregated to reduce the inherent uncertainty.

Evidential Deep Learning: Most deep learning methods utilize a softmax layer for the predictive output, but they fail to estimate predictive uncertainty. In contrast, evidential deep learning, which incorporates uncertainty estimation, can be a preferred alternative. For a q -class classification problem, SL aims to assign a belief mass to each class label and an overall uncertainty mass to the whole framework, which, for the i -th view, is formulated as the following equation with $q + 1$ mass values:

$$u^i + \sum_{k=1}^q b_k^i = 1, \quad (5)$$

where u^i and b_k^i denote the overall uncertainty and the probability for the k -th class, respectively, and they are all non-negative.

SL defines the relationship between the evidence $\mathbf{e}^i = [e_1^i, \dots, e_q^i]$ and the parameters of the Dirichlet distribution $\boldsymbol{\alpha}^i = [\alpha_1^i, \dots, \alpha_q^i]$. Specifically, the parameter α_k^i of the Dirichlet distribution is induced from e_k^i , such that $\alpha_k^i = e_k^i + 1$. Then, the belief mass b_k^i and the uncertainty u^i are calculated by

$$b_k^i = \frac{e_k^i}{S^i} = \frac{\alpha_k^i - 1}{S^i} \quad \text{and} \quad u^i = \frac{q}{S^i}, \quad (6)$$

where $S^i = \sum_{k=1}^q (e_k^i + 1) = \sum_{k=1}^q \alpha_k^i$ denotes the Dirichlet strength. Eq. (6) reflects two observations: First, the more evidence gathered for the k -th category, the higher the probability assigned to the k -th class. Second, the less total evidence observed, the greater the overall uncertainty.

To better illustrate the concepts of evidence theory, let's delve into a three-class classification example. Fig. 3(a) represents the probability space (standard 2-simplex) for a three-class problem. Consider a high-confidence classification case where the network collects evidence $\mathbf{e}_j^i = \{19, 1, 1\}$, aligning with a Dirichlet distribution having parameters $\boldsymbol{\alpha}_j^i = \{20, 2, 2\}$. Here, the uncertainty mass $u \approx 0.13$. As seen in Fig. 3(b), this results in a distribution pattern concentrated near one vertex of the triangle. Alternatively, consider the case where the evidence for each class is relatively small, such that $\mathbf{e}_j^i = \{1, 1, 1\}$. This results in parameters $\boldsymbol{\alpha}_j^i = \{2, 2, 2\}$ and an uncertainty mass $u \approx 0.5$. Fig. 3(c) illustrates how this evidence leads to a more dispersed distribution across the simplex. We also consider the case where $\mathbf{e}_j^i = \{4, 4, 4\}$, which corresponds to Dirichlet distribution parameters $\boldsymbol{\alpha}_j^i = \{5, 5, 5\}$ and an uncertainty mass of $u \approx 0.2$. As shown in Fig. 3(d), compared to the previous cases, this distribution is more focused towards the center of the simplex, indicating that an increase in evidence amount leads to reduced overall uncertainty.

Opinion Aggregation: The result obtained from Eq. (6) can be considered a subjective opinion. For each view, we have two opinions for common and specific information, denoted as $\mathcal{M}_c = \{\{b_{c,k}\}_{k=1}^q, u_c\}$ and $\mathcal{M}_s = \{\{b_{s,k}\}_{k=1}^q, u_s\}$,

respectively. These two opinions need to be aggregated. Previous works have presented several advancements in opinion aggregation. In this paper, we select the latest state-of-the-art aggregation method, as reported in [16], which enables conflicting opinion aggregation. Readers are encouraged to refer to the corresponding literature for details. Upon obtaining the aggregated opinion $\mathcal{M} = \{\{b_k\}_{k=1}^q, u\}$, we can inversely recover the corresponding evidence.

C. Inter-view Aggregation

Existing trusted multi-view learning methods treat all views equally, leading to suboptimal opinion aggregation among views. This can result in the model being less effective at distinguishing between more and less relevant views, potentially weakening the impact of important views and their corresponding evidence, thereby reducing overall performance. To address this, we incorporate an attention mechanism for inter-view aggregation to capture importance scores from other views, enhancing the evidence from high-quality views. The implementation procedures of inter-view aggregation is shown in Fig. 5.

Since we have learned both common and specific information for each view, it is more effective to combine these to represent the view information. Thus, the i -th view is represented by a common feature c and a view-specific feature s^i , denoted as $c + s^i$ with size of $l \times 1$. The corresponding query Q is then defined by:

$$Q = W^Q F_{cs}, \quad (7)$$

where $W^Q \in \mathbb{R}^{v \times v}$ denotes the query weight matrix, and $F_{cs} = [c + s^1, c + s^2, \dots, c + s^v]^T \in \mathbb{R}^{v \times l}$. We then define the update for the key K as follows:

$$K = W^K F_{cs}, \quad (8)$$

where $W^K \in \mathbb{R}^{v \times v}$ is the key weight matrix. Given that our purpose is to dynamically select the most favorable evidence for classification, the value V should be evidence-related and is defined as:

$$V = W^V E, \quad (9)$$

where $W^V \in \mathbb{R}^{v \times v}$ is the value weight matrix, and $E = [e^1, e^2, \dots, e^v]^T \in \mathbb{R}^{v \times q}$ denotes the evidence matrix.

Conventional attention mechanisms use a softmax function for dynamic weight selection. However, applying softmax in this context can cause the network to overly rely on evidence from a single view, as the weights for other views may approach zero. This leads to overconfidence in one view and hinders the effective utilization of information from all views. To address this, we adopt the ReLU activation function to achieve more balanced and reasonable weight selection. With attention considered, we can calculate the evidence for the i -th view by

$$\text{Attention}(Q^i, K, V) = \frac{\text{ReLU}\left(Q^i K^T / \sqrt{l}\right) + \epsilon}{\text{sum}\left(\text{ReLU}\left(Q^i K^T / \sqrt{l}\right) + \epsilon\right)} V, \quad (10)$$

where Q^i represents the i -th row of Q , and ϵ is a small value added to prevent division by zero.

After obtaining the attention scores for each view, the importance of evidence from high-quality views is enhanced, while that from less significant views is reduced. This approach allows the model to focus more on critical evidence that significantly influences decision-making. Subsequently, we perform opinion aggregation between views using the aforementioned conflicting opinion strategy.

D. Loss Function

The overall loss function is composed of three parts: extraction of common and specific information, intra-view aggregation, and inter-view aggregation. In the earlier subsection, we have introduced the loss functions for learning common and specific information, namely \mathcal{L}_{com} and \mathcal{L}_{spe} . Therefore, in this section, we focus on the details of the loss functions for intra-view and inter-view aggregation.

Before proceeding, we need to introduce some fundamental concepts related to designing loss functions in evidential deep learning. In this context, the softmax layer of a neural network is replaced with an activation function layer (i.e., ReLU) to ensure that the network outputs non-negative values, which are interpreted as the evidence vector. When designing the classification loss in trusted multi-view learning, the traditional cross-entropy loss must be adapted to align with the evidence-based approach in the case of j -th instance for k -th class:

$$\begin{aligned} \mathcal{L}_{acc}(\alpha_j) &= \int \left[\sum_{k=1}^q -y_{jk} \log p_{jk} \right] \frac{\prod_{k=1}^q p_{jk}^{\alpha_{jk}-1}}{B(\alpha_j)} dp_j \\ &= \sum_{k=1}^q y_{jk} (\psi(S_j) - \psi(\alpha_{jk})), \end{aligned} \quad (11)$$

where α_j denotes the parameter vector (i.e., $\alpha_j^i = e_j^i + 1$) of the Dirichlet distribution, and $\psi(\cdot)$ represents the digamma function. The above loss function ensures that the correct label of each sample generates more evidence than other classes. However, it does not guarantee that less evidence will be generated for incorrect labels. To compensate this drawback, an additional Kullback-Leibler (KL) divergence term is required:

$$\begin{aligned} \mathcal{L}_{KL}(\alpha_j) &= KL [D(\mathbf{p}_j | \tilde{\alpha}_j) || D(\mathbf{p}_j | \mathbf{1})] \\ &= \log \left(\frac{\Gamma(\sum_{k=1}^q \tilde{\alpha}_{jk})}{\Gamma(q) \prod_{k=1}^q \Gamma(\tilde{\alpha}_{jk})} \right) \\ &\quad + \sum_{k=1}^q (\tilde{\alpha}_{jk} - 1) \left[\psi(\tilde{\alpha}_{jk}) - \psi \left(\sum_{m=1}^q \tilde{\alpha}_{jm} \right) \right], \end{aligned} \quad (12)$$

where $D(\mathbf{p}_j | \mathbf{1})$ is the uniform Dirichlet distribution, $\tilde{\alpha}_j = y_j + (1 - y_j) \odot \alpha_j$ is the Dirichlet parameter that prevents the evidence for the ground truth class from being penalized to zero, and $\Gamma(\cdot)$ stands for gamma function. Combining (11) and (12), we have

$$\mathcal{L}_{acc}(\alpha_j) = \mathcal{L}_{acc}(\alpha_j) + \lambda_t \mathcal{L}_{KL}(\alpha_j), \quad (13)$$

where λ_t is a positive balance factor with t being the current training epoch index.

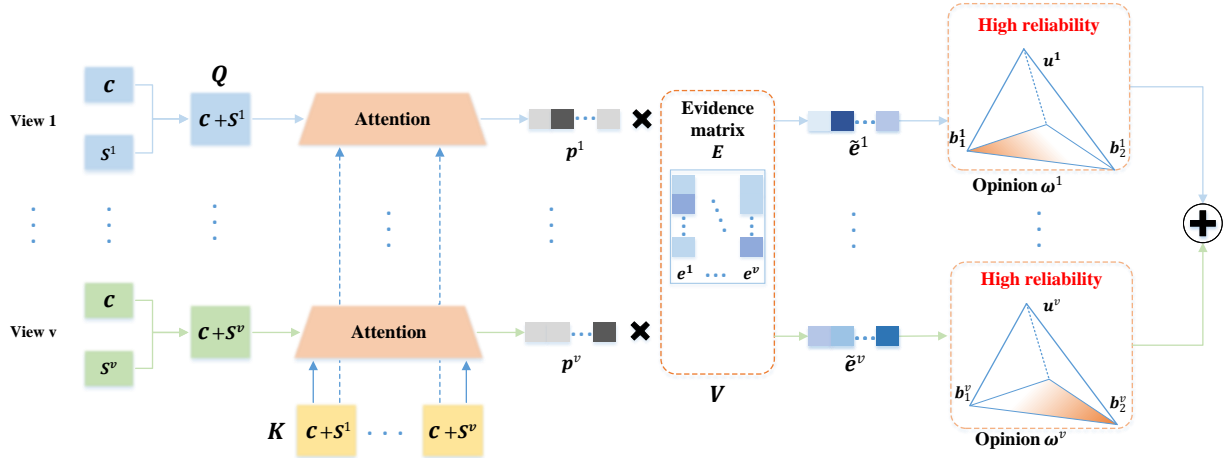


Fig. 5. Structure of inter-view aggregation. An attention mechanism at the evidence level is designed to enhance the importance of high-quality evidence.

In the intra-view aggregation (i.e., $H1$ hierarchy), apart from the basic classification loss $\mathcal{L}_{acc}(\alpha_j^i)$, we also hope that the extracted common and specific information can guide correct classification. To achieve this, we incorporate cross-entropy losses for the common and specific information, denoted as $\mathcal{L}_{acc}(\alpha_{c,j})$ and $\mathcal{L}_{acc}(\alpha_{s,j}^i)$, respectively. Since our model employs a conflictive opinion aggregation strategy, there is an additional loss term for the degree of conflict between common and specific components. Therefore, the loss for $H1$ is given by

$$\mathcal{L}_{H1} = \frac{1}{v} \sum_{i=1}^v [\mathcal{L}_{acc}(\alpha_j^i) + (\mathcal{L}_{acc}(\alpha_{c,j}) + \mathcal{L}_{acc}(\alpha_{s,j}^i))] + \gamma C(\omega_{c,j}, \omega_{s,j}^i), \quad (14)$$

where $C(\omega_{c,j}, \omega_{s,j}^i)$ characterizes the degree of conflict between common and specific components with the corresponding calculation detailed in [14], and γ is a trade-off parameter.

In the inter-view aggregation (i.e., $H2$ hierarchy), we use (13) for the basic classification loss. Additionally, we aim for the attention-induced views to achieve reliable classification, so we introduce an extra classification loss for these views. Furthermore, we account for the conflict degree loss between views. Thus, we have

$$\mathcal{L}_{H2} = \mathcal{L}_{acc}(\alpha_j) + \sum_{i=1}^v \mathcal{L}_{acc}(\hat{\alpha}_j^i) + \gamma \mathcal{L}_{con}, \quad (15)$$

where $\hat{\alpha}_j$ is the parameter vector of the Dirichlet distribution after applying attention, and \mathcal{L}_{con} is given by

$$\mathcal{L}_{con} = \frac{1}{v-1} \sum_{p=1}^v \left(\sum_{q \neq p}^v C(\omega_j^p, \omega_j^q) \right). \quad (16)$$

In summary, the overall loss of our model is shown as:

$$\mathcal{L}_{overall} = \mathcal{L}_{H1} + \mathcal{L}_{H2} + \delta \mathcal{L}_{com} + \eta \mathcal{L}_{spe}, \quad (17)$$

where δ and η are trade-off parameters. The implementation pseudocode of our model is summarized in **Algorithm 1**.

Algorithm 1 Implementation pseudocode of GTMC-HOA

Input: Multi-view dataset: $\{X^i, y\}_{i=1}^v$

Parameter: Hyper-parameter: $l = 64, \gamma = 1, \delta = 1, \eta = \{0.1, 0.01, 0.001\}$

—Train—

Output: Network's parameters.

01: **while** not converged **do**

02: Initialize common features c .

03: **for** $i = 1 : v$ **do**

04: $c^i \leftarrow$ common subspace network output.

05: $s^i \leftarrow$ specific information network output.

06: Calculate $c = c + c^i$.

07: Calculate common information $c = c/v$.

08: **for** $i = 1 : v$ **do**

09: $e_c, e_s^i \leftarrow$ evidential network output.

10: Calculate e^i by Intra-view Aggregation.

11: **for** $i = 1 : v$ **do**

12: Calculate \hat{e}^i by Inter-view Aggregation.

13: Calculate distribution $\hat{\alpha}^i = \hat{e}^i + 1$.

14: Calculate the joint distribution α .

15: Calculate the overall loss $\mathcal{L}_{overall}$ by Eq. (17).

16: Update the networks by gradient descent.

17: **end while**

18: **return** networks parameters.

—Test—

Output: The final prediction and corresponding uncertainty.

01: Repeat training steps 02-14.

02: Calculate the joint b, u by Eq. 6.

03: **return** the decision b and associated uncertainty u .

IV. EXPERIMENTS

In this section, we compare the classification accuracy of GTMC-HOA with existing state-of-the-art methods, and investigate the model robustness against varying noise. We conduct an ablation study to figure out the contributions of main modules. Moreover, we analyze the conflictive degree,

as well as the local and overall uncertainty on conflictive multi-view data.

A. Experimental Setup

1) *Datasets*: **HandWritten**¹ comprises 2000 instances of handwritten numerals ranging from ‘0’ to ‘9’, with 200 patterns per class. It is represented using six feature sets. **CUB**² consists of 11788 instances associated with text descriptions of 200 different categories of birds. In this paper, we focus on the first 10 categories and extract image features using GoogleNet and corresponding text features using doc2vec. **Scene15**³ includes 4485 images from 15 indoor and outdoor scene categories. We extract three types of features GIST, PHOG, and LBP. **PIE**⁴ contains 680 instances belonging to 68 classes. We extract intensity, LBP, and Gabor as 3 views. **Caltech101**⁵ comprises 8677 images from 101 classes. We select 2386 samples from 20 classes, where each image has six features: Gabor, Wavelet Moments, CENTRIST, HOG, GIST, and LBP. **NUS-WIDE**⁶ consists of 269648 images with 81 concepts. For the top 12 classes, we select 200 images from each class, with a total of 6 different views. Table I presents the details of datasets.

TABLE I
DATASET SUMMARY.

Dataset	Size	K	Dimensionality
HandWritten	2000	10	240/76/216/47/64/6
CUB	600	10	1024/300
Scene15	4485	15	20/59/40
PIE	680	68	484/256/279
Caltech101	2386	20	48/40/254/1984/512/928
NUS-WIDE	2400	12	64/144/73/128/225/500

2) *Compared Methods*: The compared methods involve feature fusion and decision fusion baselines. Specifically, 1) feature fusion baselines include: **CPM-Nets** (Cross Partial Multi-view Networks) [49] is a multi-view feature fusion method designed to learn versatile representations that handle complex correlations across different views. **DUA-Nets** (Dynamic Uncertainty-Aware Networks) [50] is an uncertainty-aware method, that uses reversal networks to integrate intrinsic information from different views into a unified representation. **EDL** (Evidential Deep Learning) [38] designs the predictive distribution of the classification by placing a Dirichlet distribution on the class probabilities. 2) Decision fusion baselines include: **TMC** (Trusted Multi-view Classification) [12] addresses the uncertainty estimation problem and formulates a reliable classification framework. **ECML** (Evidential Conflictive Multi-view Learning) [14] puts forward a conflictive opinion aggregation model.

3) *Implementation Details*: For all datasets, we randomly select 80% of the samples for the training set and use the remaining 20% for the test set. For our algorithm, the Adam optimizer is used to train the network, where l_2 -norm regularization is set to $1e^{-5}$. We employ 5-fold cross-validation to select the learning rate from $\{1e^{-4}, 3e^{-4}, 1e^{-3}, 3e^{-3}\}$. For selecting the dimension l of the shared subspace of our model, we conduct accuracy comparison experiments with respect to dimension on the Scene15 dataset, while maintaining other parameters unchanged. The results on both normal and conflictive scenarios are shown in Fig. 6. It is seen that the model’s accuracy initially increases with l but eventually declines. While higher dimensions can enhance performance, they also significantly increase complexity. For example, the model’s parameter file size grows from 158KB at $l = 64$ to 52008KB at $l = 2048$, reflecting a huge increase in complexity. Therefore, we choose $l = 64$ for our model to make a trade-off between accuracy and computational cost. For other hyperparameters, both δ and γ on all datasets are set to 1. Due to the diverse data features from different datasets, the parameter η is selected from $\{0.1, 0.01, 0.001\}$.

To generate a test set containing conflicting instances, we perform the following operations: (1) For noisy views, we add Gaussian noise with a fixed standard deviation σ to 10% of the test instances. (2) For unaligned views, we select 40% of the test instances and modify the information in a random view, resulting in a misalignment between the label of that view and the true label of the instance. All methods are implemented by PyTorch on a NVIDIA GeForce RTX 4080 with GPU of 16GB memory. Experimental results are reported by averaging 10 independent trials.

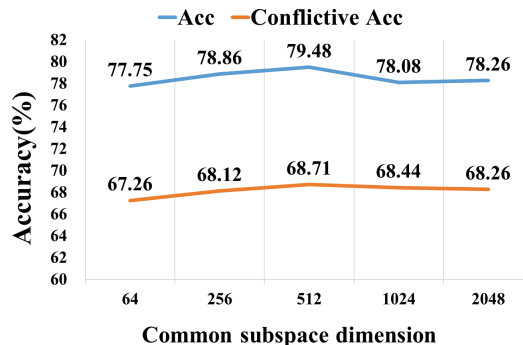


Fig. 6. Accuracy comparison with respect to l .

B. Experimental Results

1) *Accuracy Comparison*: Table II records the comparison results of various methods on normal and conflictive test sets. It is observed that CPM-Nets encounters a significant decline in performance on conflictive test sets compared to normal test sets, exemplified by a 35.88% drop on the PIE dataset. This is because CPM-Nets cannot assess the quality of view data. In contrast, evidence theory-based methods demonstrate a certain ability to maintain performance on conflictive test sets, which is particularly evident for ECML and our GTMC-HOA. For instance, GTMC-HOA shows a decline of no more

¹<https://archive.ics.uci.edu/ml/datasets/Multiple+Features>

²<http://www.vision.caltech.edu/visipedia/CUB-200.html>

³<https://doi.org/10.6084/m9.figshare.7007177.v1>

⁴http://www.cs.cmu.edu/afs/cs/project/PIE/MultiPie/MultiPie_Home.html

⁵http://www.vision.caltech.edu/Image_Datasets/Caltech101

⁶<https://paperswithcode.com/dataset/nus-wide>

TABLE II
ACCURACY (%) ON NORMAL AND CONFLICTIVE TEST SETS. THE BEST RESULTS ARE HIGHLIGHTED IN BOLD, WHILE THE SECOND-BEST ARE UNDERLINED.

Datasets	Test sets	CPM-Nets	DUA-Nets	EDL	TMC	ECML	Ours
HandWritten	Normal	94.60±0.57	97.30±0.77	97.05±0.50	<u>97.57±0.17</u>	97.16±0.15	98.48 ± 0.12
	Conflictive	83.93±0.86	87.16±0.34	89.60±0.62	92.02±0.30	92.69±0.20	94.65 ± 0.37
CUB	Normal	88.75±0.93	80.33±1.25	89.22±1.12	90.78±0.43	<u>92.00±0.37</u>	92.48 ± 0.30
	Conflictive	68.55±1.10	54.92±4.12	70.79±0.91	<u>73.13±0.45</u>	73.30±1.21	73.02 ± 0.96
Scene15	Normal	59.06±1.11	68.23±0.11	46.84±0.73	67.35±0.18	70.80±0.16	77.75 ± 0.28
	Conflictive	28.25±1.48	27.45±1.90	36.68±0.72	42.92±0.35	<u>55.63±0.45</u>	67.26 ± 0.43
PIE	Normal	88.68±0.82	82.66±2.02	82.64±0.94	91.91±0.43	94.11±0.68	<u>93.13 ± 0.50</u>
	Conflictive	52.80±1.59	57.57±3.09	59.50±1.64	68.55±1.79	81.94±0.66	83.13 ± 0.95
Caltech101	Normal	87.87±0.91	83.47±1.66	88.20±0.67	90.55±0.29	<u>91.13±1.61</u>	93.61 ± 0.20
	Conflictive	64.56±0.51	78.47±1.92	84.14±0.34	87.25±0.34	<u>89.01±0.52</u>	89.83 ± 0.31
NUS-WIDE	Normal	36.44±1.18	34.40±1.48	36.00±0.60	40.44±0.61	<u>42.97±0.54</u>	47.72 ± 0.56
	Conflictive	24.98±1.07	31.81±2.41	31.79±0.58	33.25±0.57	<u>37.95±0.40</u>	44.59 ± 0.37

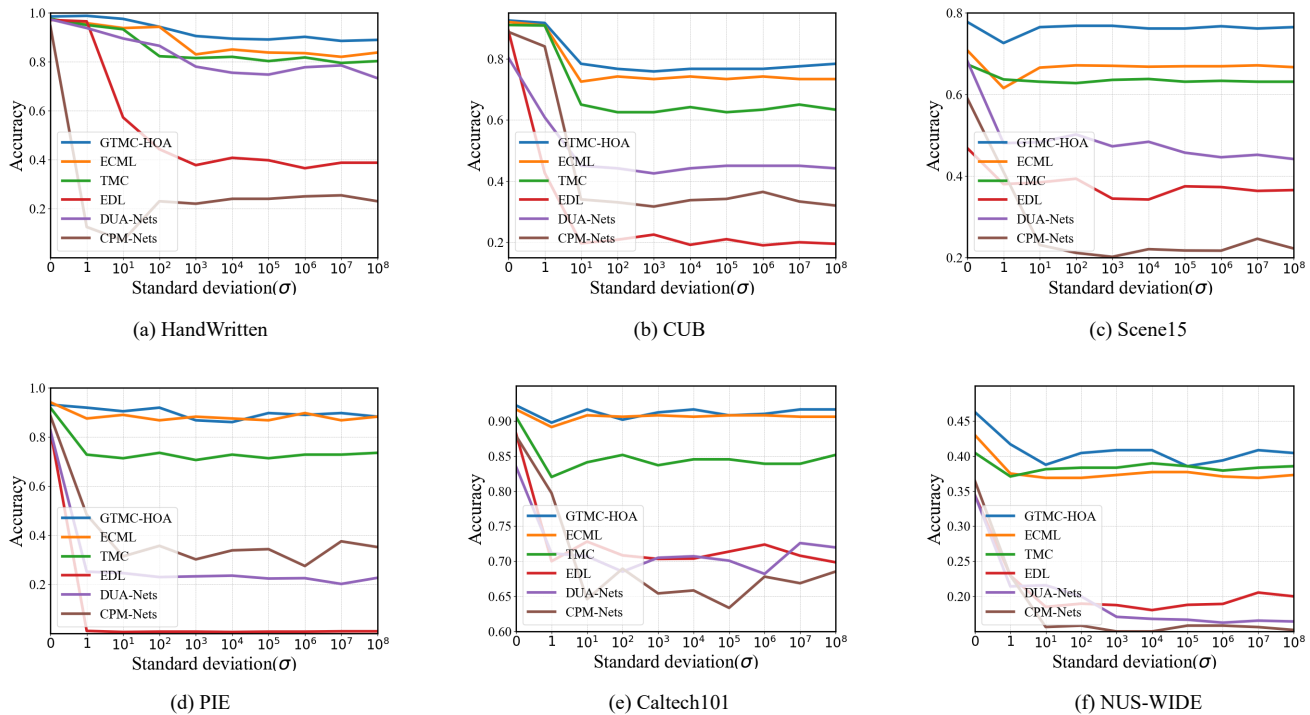


Fig. 7. Performance comparison on different datasets with varying noise levels.

than 10% on most datasets, except for the CUB dataset, where the decline reaches approximately 20%. This is attributed to CUB being a small-scale dataset with only two views, making it challenging for the model to conduct sufficient training to handle conflictive data.

Importantly, we see that our proposed GTMC-HOA nearly outperforms all other baselines on both normal and conflictive test sets. For example, on normal test sets, GTMC-HOA outperforms other methods on the HandWritten, CUB, Scene15, Caltech101, and NUS-WIDE datasets. Notably, GTMC-HOA achieves a significant performance increase of 6.95% on the Scene15 dataset compared to ECML, the second-best performing method. We argue that this is because the intra-view aggregation improves the view quality and reliability, which can be further supported in the uncertainty estimation study.

2) *Performance Evaluation with Varying Noise Levels:* To further demonstrate the superiority of our GTMC-HOA model

in the presence of noise, we conduct comparison experiments by adding Gaussian noise with different variances to the test data. Specifically, we randomly add Gaussian noise to approximately half of the views for all datasets, and the noise intensity, characterized by its standard deviation, ranges from $\{10^0, 10^1, \dots, 10^8\}$. Fig. 7 shows the comparison results on six datasets with varying noise levels. It is observed that in the absence of Gaussian noise, GTMC-HOA outperforms other models. All tested models inevitably experience a decline after adding noise. It is worth noting that CPM-Nets and EDL exhibit a significant decline in performance in the presence of noise, especially when compared to TMC, ECML, and GTMC-HOA. This disparity arises because CPM-Nets is not based on evidence theory and thus cannot evaluate the uncertainty of noisy views, while EDL, being a single-view model, lacks the advantage of multi-view models that can mitigate noisy

view limitations by leveraging information from other reliable views. Furthermore, we observe that model performance tends to stabilize at a certain accuracy level when noise intensity reaches a specific threshold. Importantly, compared to the latest trusted methods, namely TMC and ECML, our GTMC-HOA model demonstrates clear superiority across all tested datasets under the same noise level. This is due to the proposed hierarchical aggregation framework, which enhances uncertainty awareness in both intra- and inter-view opinion aggregation, thereby improving the reliability of decision-making.

3) *Confictive Degree Visualization*: Fig. 8 presents the conflictive degree result on the HandWritten dataset. To introduce conflicts, we modify the content in the first view, resulting in misalignment with the content from the other views. We observe and analyze the following: (1) The first view exhibits the highest level of conflict with other views, demonstrating that GTMC-HOA effectively captures conflict degrees among views. (2) The remaining view pairs, excluding those involving the first view, also show certain conflict degrees. This is because our model extracts common features across views, causing the conflictive information from one view to influence the others.

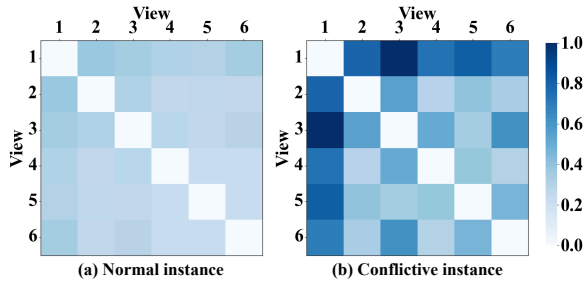


Fig. 8. Conflictive degree visualization. (a) conflictive degree of normal instances, (b) conflictive degree of conflictive instances.

4) *Ablation Study*: We conduct ablation experiments to investigate the contributions of $H1$ and $H2$ hierarchy aggregations, as shown in Fig. 9. In the first test, we remove the $H1$ hierarchy aggregation, and in the second, we exclude the attention mechanism of the $H2$ hierarchy aggregation. These two variants are denoted as GTMC-HOA-v1 and GTMC-HOA-v2, respectively. Our results indicate that both intra-view and inter-view aggregations contribute to overall performance. In particular, removing the first hierarchy of aggregation leads to a more significant performance decline, highlighting the importance of intra-view aggregation.

5) *Uncertainty Estimation*: To evaluate the estimated uncertainty, we visualize the distribution of normal and conflictive test sets for both intra-view and inter-view aggregation. The distribution from intra-view aggregation represents local uncertainty, while the distribution from inter-view aggregation reflects overall uncertainty. Experiments are conducted on the CUB dataset, with conflictive test sets created by adding Gaussian noise with standard deviations of $\sigma = 0.1, 1, 5, 10$ to 50% of the test instances, as shown in Figs. 10 and 11. It is observed that, in both cases, the distribution curves of conflictive instances deviate more from those of normal

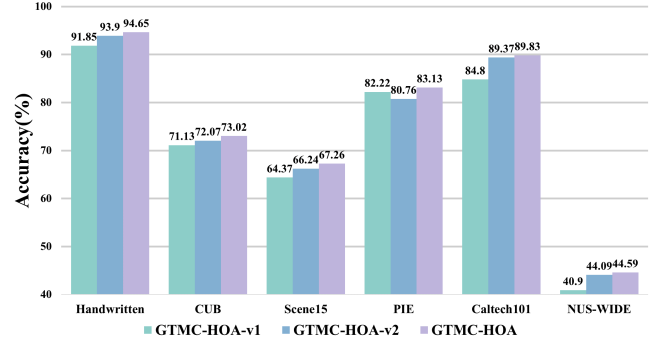


Fig. 9. Ablation study.

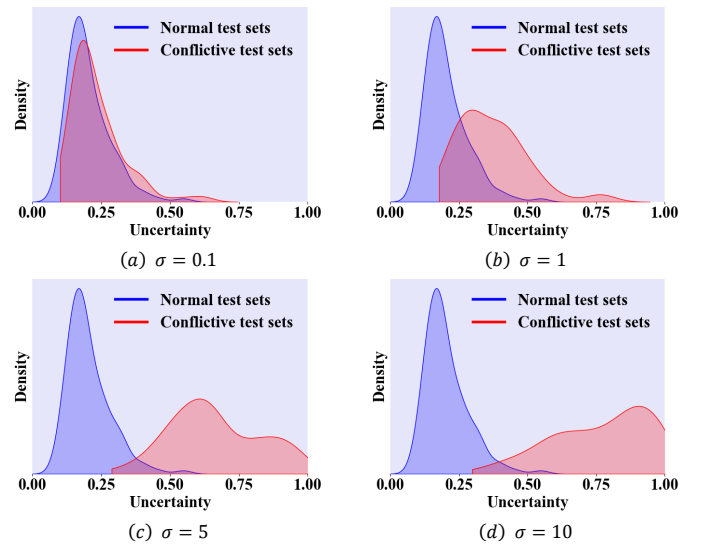


Fig. 10. Density of local uncertainty.

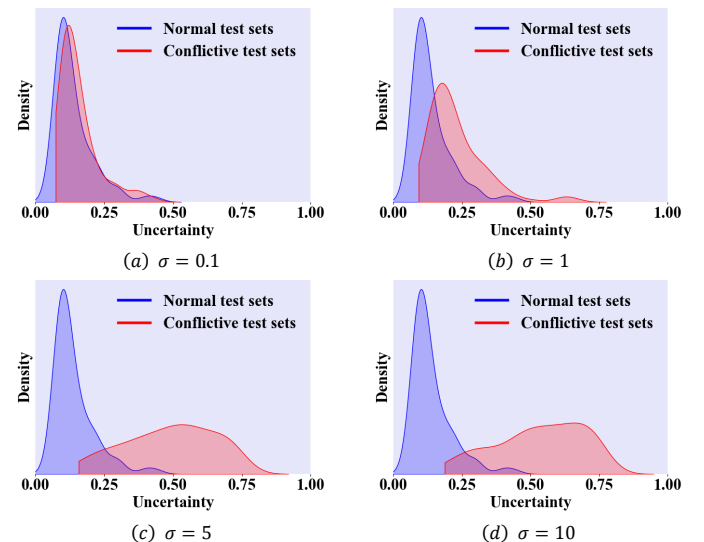


Fig. 11. Density of overall uncertainty.

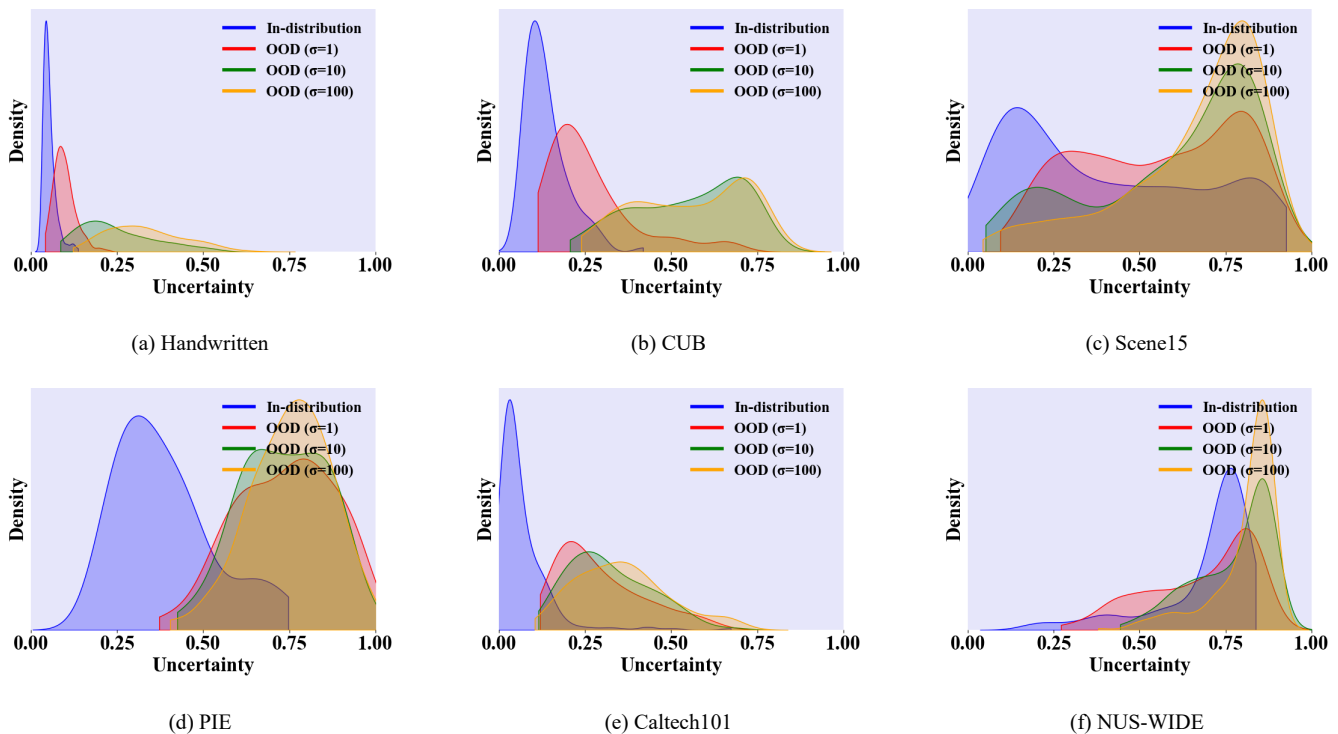


Fig. 12. Density of uncertainty obtained on different datasets.

instances as noise intensity increases. Moreover, by comparing Fig. 10(a) with 11(a), both under the same noise intensity of σ , we find that the distribution curve of overall uncertainty shifts to the left compared to that of local uncertainty. This shift implies a reduction in uncertainty after the second hierarchy of aggregation.

In addition, we conduct more experiments regarding uncertainty estimation on different datasets, as shown in Fig. 12. We have similar observations as described above. These observations indicate that both hierarchies of aggregation effectively estimate uncertainty, thereby improving view quality and overall reliability.

V. CONCLUSIONS

In this paper, we proposed a hierarchical opinion aggregation framework for trusted multi-view classification, namely GTMC-HOA. GTMC-HOA is composed of two hierarchies of aggregation: intra-view and inter-view aggregation. The intra-view aggregation is realized by first learning common and view-specific information, and then aggregate them together based on a trusted strategy. This hierarchy of aggregation helps to reduce feature noise and improve view quality. The inter-view aggregation incorporates an attention mechanism to determine attention scores among views, which guides more accurate opinion aggregation across views. Experimental results on six datasets confirmed the superiority of GTMC-HOA.

REFERENCES

- [1] H. Gao, F. Nie, X. Li, and H. Huang, "Multi-view subspace clustering," in *Proceedings of the IEEE International Conference on Computer Vision*, 2015, pp. 4238–4246.
- [2] L. Cao, L. Shi, J. Wang, Z. Yang, and B. Chen, "Robust subspace clustering by logarithmic hyperbolic cosine function," *IEEE Signal Processing Letters*, vol. 30, pp. 508–512, 2023.
- [3] H. Wang, Y. Yang, and B. Liu, "Gmc: Graph-based multi-view clustering," *IEEE Transactions on Knowledge and Data Engineering*, vol. 32, no. 6, pp. 1116–1129, 2019.
- [4] J. Wen, K. Yan, Z. Zhang, Y. Xu, J. Wang, L. Fei, and B. Zhang, "Adaptive graph completion based incomplete multi-view clustering," *IEEE Transactions on Multimedia*, vol. 23, pp. 2493–2504, 2020.
- [5] Q. Wang, J. Cheng, Q. Gao, G. Zhao, and L. Jiao, "Deep multi-view subspace clustering with unified and discriminative learning," *IEEE Transactions on Multimedia*, vol. 23, pp. 3483–3493, 2020.
- [6] X. Yan, S. Hu, Y. Mao, Y. Ye, and H. Yu, "Deep multi-view learning methods: A review," *Neurocomputing*, vol. 448, pp. 106–129, 2021.
- [7] M. Kan, S. Shan, and X. Chen, "Multi-view deep network for cross-view classification," in *Proceedings of the IEEE Conference on Computer Vision and Pattern Recognition*, 2016, pp. 4847–4855.
- [8] S. Wang, X. Liu, X. Zhu, P. Zhang, Y. Zhang, F. Gao, and E. Zhu, "Fast parameter-free multi-view subspace clustering with consensus anchor guidance," *IEEE Transactions on Image Processing*, vol. 31, pp. 556–568, 2021.
- [9] Y. Lee, Y. Jeong, K. Park, and S. Kang, "Mvifs: Multi-view feature selection for recommender system," in *Proceedings of the 32nd ACM International Conference on Information and Knowledge Management*, 2023, pp. 4048–4052.
- [10] Y. Wang, X. Lin, L. Wu, W. Zhang, Q. Zhang, and X. Huang, "Robust subspace clustering for multi-view data by exploiting correlation consensus," *IEEE Transactions on Image Processing*, vol. 24, no. 11, pp. 3939–3949, 2015.
- [11] S. Luo, C. Zhang, W. Zhang, and X. Cao, "Consistent and specific multi-view subspace clustering," in *Proceedings of the AAAI Conference on Artificial Intelligence*, vol. 32, no. 1, 2018.
- [12] Z. Han, C. Zhang, H. Fu, and J. T. Zhou, "Trusted multi-view classification with dynamic evidential fusion," *IEEE Transactions on Pattern Analysis and Machine Intelligence*, vol. 45, no. 2, pp. 2551–2566, 2022.
- [13] G. Shafer, *A mathematical theory of evidence*. Princeton University Press, 1976, vol. 42.
- [14] C. Xu, J. Si, Z. Guan, W. Zhao, Y. Wu, and X. Gao, "Reliable conflictive multi-view learning," in *Proceedings of the AAAI Conference on Artificial Intelligence*, vol. 38, no. 14, 2024, pp. 16 129–16 137.
- [15] W. Liu, X. Yue, Y. Chen, and T. Denooux, "Trusted multi-view deep

- learning with opinion aggregation,” in *Proceedings of the AAAI Conference on Artificial Intelligence*, vol. 36, no. 7, 2022, pp. 7585–7593.
- [16] C. Xu, Y. Zhang, Z. Guan, and W. Zhao, “Trusted multi-view learning with label noise,” *arXiv preprint arXiv:2404.11944*, 2024.
- [17] L. Shi, L. Cao, Z. Chen, Y. Zhao, and B. Chen, “Nonlinear subspace clustering by functional link neural networks,” *Applied Soft Computing*, p. 112303, 2024.
- [18] M. Brbić and I. Kopriva, “Multi-view low-rank sparse subspace clustering,” *Pattern Recognition*, vol. 73, pp. 247–258, 2018.
- [19] C. Zhang, H. Fu, Q. Hu, X. Cao, Y. Xie, D. Tao, and D. Xu, “Generalized latent multi-view subspace clustering,” *IEEE Transactions on Pattern Analysis and Machine Intelligence*, vol. 42, no. 1, pp. 86–99, 2018.
- [20] M.-S. Chen, L. Huang, C.-D. Wang, and D. Huang, “Multi-view clustering in latent embedding space,” in *Proceedings of the AAAI Conference on Artificial Intelligence*, vol. 34, no. 04, 2020, pp. 3513–3520.
- [21] L. Shi, L. Cao, J. Wang, and B. Chen, “Enhanced latent multi-view subspace clustering,” *IEEE Transactions on Circuits and Systems for Video Technology*, 2024.
- [22] T. Wu, S. Feng, and J. Yuan, “Low-rank kernel tensor learning for incomplete multi-view clustering,” in *Proceedings of the AAAI Conference on Artificial Intelligence*, vol. 38, no. 14, 2024, pp. 15952–15960.
- [23] X. Liu, X. Zhu, M. Li, L. Wang, E. Zhu, T. Liu, M. Kloft, D. Shen, J. Yin, and W. Gao, “Multiple kernel k -means with incomplete kernels,” *IEEE Transactions on Pattern Analysis and Machine Intelligence*, vol. 42, no. 5, pp. 1191–1204, 2019.
- [24] J. Liu, X. Liu, J. Xiong, Q. Liao, S. Zhou, S. Wang, and Y. Yang, “Optimal neighborhood multiple kernel clustering with adaptive local kernels,” *IEEE Transactions on Knowledge and Data Engineering*, vol. 34, no. 6, pp. 2872–2885, 2020.
- [25] Y. Xie, D. Tao, W. Zhang, Y. Liu, L. Zhang, and Y. Qu, “On unifying multi-view self-representations for clustering by tensor multi-rank minimization,” *International Journal of Computer Vision*, vol. 126, pp. 1157–1179, 2018.
- [26] J. Wu, X. Xie, L. Nie, Z. Lin, and H. Zha, “Unified graph and low-rank tensor learning for multi-view clustering,” in *Proceedings of the AAAI Conference on Artificial Intelligence*, vol. 34, no. 04, 2020, pp. 6388–6395.
- [27] Y. Qin, Z. Tang, H. Wu, and G. Feng, “Flexible tensor learning for multi-view clustering with markov chain,” *IEEE Transactions on Knowledge and Data Engineering*, 2023.
- [28] K. Zhan, F. Nie, J. Wang, and Y. Yang, “Multiview consensus graph clustering,” *IEEE Transactions on Image Processing*, vol. 28, no. 3, pp. 1261–1270, 2018.
- [29] Z. Li, C. Tang, X. Liu, X. Zheng, W. Zhang, and E. Zhu, “Consensus graph learning for multi-view clustering,” *IEEE Transactions on Multimedia*, vol. 24, pp. 2461–2472, 2021.
- [30] H. Wang, G. Jiang, J. Peng, R. Deng, and X. Fu, “Towards adaptive consensus graph: multi-view clustering via graph collaboration,” *IEEE Transactions on Multimedia*, vol. 25, pp. 6629–6641, 2022.
- [31] W. K. Wong, N. Han, X. Fang, S. Zhan, and J. Wen, “Clustering structure-induced robust multi-view graph recovery,” *IEEE Transactions on Circuits and Systems for Video Technology*, vol. 30, no. 10, pp. 3584–3597, 2019.
- [32] Z. Lin, Z. Kang, L. Zhang, and L. Tian, “Multi-view attributed graph clustering,” *IEEE Transactions on Knowledge and Data Engineering*, vol. 35, no. 2, pp. 1872–1880, 2021.
- [33] Z. Lin and Z. Kang, “Graph filter-based multi-view attributed graph clustering,” in *IJCAI*, 2021, pp. 2723–2729.
- [34] J. Chen, H. Mao, W. L. Woo, and X. Peng, “Deep multiview clustering by contrasting cluster assignments,” in *Proceedings of the IEEE/CVF International Conference on Computer Vision*, 2023, pp. 16 752–16 761.
- [35] Y. Lu, Y. Lin, M. Yang, D. Peng, P. Hu, and X. Peng, “Decoupled contrastive multi-view clustering with high-order random walks,” in *Proceedings of the AAAI Conference on Artificial Intelligence*, vol. 38, no. 13, 2024, pp. 14 193–14 201.
- [36] C. Liu, J. Wen, X. Luo, and Y. Xu, “Incomplete multi-view multi-label learning via label-guided masked view-and category-aware transformers,” in *Proceedings of the AAAI Conference on Artificial Intelligence*, vol. 37, no. 7, 2023, pp. 8816–8824.
- [37] B. Yang, X. Zhang, J. Wu, F. Nie, Z. Lin, F. Wang, and B. Chen, “Fast multiview anchor-graph clustering,” *IEEE Transactions on Neural Networks and Learning Systems*, 2024.
- [38] M. Sensoy, L. Kaplan, and M. Kandemir, “Evidential deep learning to quantify classification uncertainty,” *Advances in Neural Information Processing Systems*, vol. 31, 2018.
- [39] Z. Han, C. Zhang, H. Fu, and J. T. Zhou, “Trusted multi-view classification,” in *International Conference on Learning Representations*, 2020.
- [40] Y. Liu, L. Liu, C. Xu, X. Song, Z. Guan, and W. Zhao, “Dynamic evidence decoupling for trusted multi-view learning,” in *ACM Multimedia 2024*.
- [41] H. Zhou, Z. Xue, Y. Liu, B. Li, J. Du, M. Liang, and Y. Qi, “Calm: An enhanced encoding and confidence evaluating framework for trustworthy multi-view learning,” in *Proceedings of the 31st ACM International Conference on Multimedia*, 2023, pp. 3108–3116.
- [42] H. Zhou, Z. Xue, Y. Liu, B. Li, J. Du, and M. Liang, “Rtmc: A robust trusted multi-view classification framework,” in *2023 IEEE International Conference on Multimedia and Expo (ICME)*. IEEE, 2023, pp. 576–581.
- [43] X. Wang, Y. Wang, Y. Wang, A. Huang, and J. Liu, “Trusted semi-supervised multi-view classification with contrastive learning,” *IEEE Transactions on Multimedia*, 2024.
- [44] S. Du, Z. Fang, S. Lan, Y. Tan, M. Günther, S. Wang, and W. Guo, “Bridging trustworthiness and open-world learning: An exploratory neural approach for enhancing interpretability, generalization, and robustness,” in *Proceedings of the 31st ACM International Conference on Multimedia*, 2023, pp. 8719–8729.
- [45] X. Zou, C. Tang, X. Zheng, Z. Li, X. He, S. An, and X. Liu, “Dpnet: Dynamic poly-attention network for trustworthy multi-modal classification,” in *Proceedings of the 31st ACM International Conference on Multimedia*, 2023, pp. 3550–3559.
- [46] P. Liu, X. Qiu, and X.-J. Huang, “Adversarial multi-task learning for text classification,” in *Proceedings of the 55th Annual Meeting of the Association for Computational Linguistics (Volume 1: Long Papers)*, 2017, pp. 1–10.
- [47] X. Wu, Q.-G. Chen, Y. Hu, D. Wang, X. Chang, X. Wang, and M.-L. Zhang, “Multi-view multi-label learning with view-specific information extraction,” in *IJCAI*, 2019, pp. 3884–3890.
- [48] A. Jsang, *Subjective Logic: A formalism for reasoning under uncertainty*. Springer Publishing Company, Incorporated, 2018.
- [49] C. Zhang, Y. Cui, Z. Han, J. T. Zhou, H. Fu, and Q. Hu, “Deep partial multi-view learning,” *IEEE Transactions on Pattern Analysis and Machine Intelligence*, vol. 44, no. 5, pp. 2402–2415, 2020.
- [50] Y. Geng, Z. Han, C. Zhang, and Q. Hu, “Uncertainty-aware multi-view representation learning,” in *Proceedings of the AAAI Conference on Artificial Intelligence*, vol. 35, no. 9, 2021, pp. 7545–7553.